Iannelli, A., Marcos, A., & Lowenberg, M. (2018). Study of Flexible Aircraft Body Freedom Flutter with Robustness Tools. *Journal of Guidance, Control, and Dynamics*, *41*(5). https://doi.org/10.2514/1.G003165

Study of Flexible Aircraft Body Freedom Flutter with Robustness Tools

Andrea Iannelli[a] and Andrés Marcos[b] and Mark Lowenberg[c]
Department of Aerospace Engineering, University of Bristol, UK

Body Freedom Flutter (BFF) is a dynamic instability featuring strong coupling between rigid-body and elastic modes of the aircraft. Flexible configurations with adverse structural and geometric properties have been found susceptible to this phenomenon. Features that complicate its study are the presence of multiple modal instabilities, and the different influence that system parameters have on each of them. The robust analysis framework based on Linear Fractional Transformation modeling and structured singular value μ analysis is used in this work to study the BFF problem in a systematic way. The analyses performed showcase the potential of these methods, not only in supplying a characterization of the system in terms of its robustness, but also in gaining further understanding of the BFF problem and reconciling the results with physical features. It is also shown that the robust modeling analysis framework complements the conventional, state of practice, methods while allowing the study of highly coupled systems (of which the flexible aircraft is an example) to be addressed in an incremental and methodological manner.

For this study a simplified wing model is augmented including the short-period approximation aircraft model and the rigid-elastic coupling terms. The proposed model captures properties and trends of both restrained wing flutter and BFF instabilities.

[a] Ph.D. Student, Aerospace Engineering Department, University Walk, Bristol BS8 1TR, UK.
[b] Senior Lecturer, Aerospace Engineering Department, University Walk, Bristol BS8 1TR, UK. Senior Member AIAA.
[c] Professor, Aerospace Engineering Department, University Walk, Bristol BS8 1TR, UK. Senior Member AIAA.

Nomenclature

h, α = Plunge and pitch degrees of freedom of the typical section, m and rad

K_h, K_α = Linear and rotational stiffness of the typical section, $\frac{N}{m^2}$ and N

m_w, m = Wing mass per unit span and total aircraft mass, $\frac{kg}{m}$ and kg

$\mathbf{X}^E$ = Vector of elastic DOFs

$\mathbf{L_a}^E$ = Aerodynamic loads on the wing due to $\mathbf{X}^E$

$\mathbf{M_s}$, $\mathbf{K_s}$ = Structural mass and stiffness matrix

$\mathbf{A}$ = Aerodynamic Influence Coefficient (AIC) matrix

q = Dynamic pressure, $\frac{N}{m^2}$

V = Airspeed, $\frac{m}{s}$

EI, GJ = Bending and torsional stiffness of the uniform wing, N.m^2

ω_b, ω_t = Uncoupled bending and torsional natural frequencies of the uniform wing, $\frac{rad}{s}$

D = Tail leading edge distance from the nose, m

L = Wing span, m

$\bar{\alpha}$, $\bar{\theta}$ = Vehicle angle of attack and pitch angle, rad

$\bar{q}$ = Vehicle pitch rate, $\frac{rad}{s}$

$\mathbf{X}^R$ = Vector of rigid DOFs

$\mathbf{L_a}^R$ = Aerodynamic loads on the wing due to $\mathbf{X}^R$

ω_{SP}, ζ_{SP} = Short-period frequency ($\frac{rad}{s}$) and damping

α_{loc} = Wing local angle of attack (including rigid and elastic effects), rad

$C_L^{w,R}$, $C_L^{w,E}$ = Wing rigid and elastic lift coefficient

V_f, ω_f = Flutter speed ($\frac{m}{s}$) and frequency ($\frac{rad}{s}$)

V_H = Aircraft tail volume

I_{yy} = Aircraft pitch moment of inertia, $kg.m^2$

EI_G = Bending stiffness of the Goland wing, $N.m^2$

σ_s = Bending stiffness factor (defining the wing bending stiffness as EI=$\sigma_s EI_G$)

δ_x, λ_x = Uncertainty parameter x and corresponding level of uncertainty

$\mathbf{\Delta}^{y,R-z,C}$ = Structured uncertainty matrix with total y real and z complex uncertainties

$\mathbf{\Delta^{cr}}$ = Smallest perturbation matrix satisfying the determinant condition

I. Introduction

Aeroelasticity investigates the coupled problem of a flexible structure surrounded by a fluid flow generating a pressure depending on its geometry. Flutter is one of the most important phenomena which can be investigated within the aeroelastic framework. This is a self-excited instability in which aerodynamic forces on a flexible body couple with its natural modes of vibration producing oscillatory motion [1]. The level of vibration may result in sufficiently large amplitudes to provoke failure and often this phenomenon dictates the design of the system.

In the aeronautical industry much analysis, at least for preliminary evaluations, relies on predictions based on *restrained* body models (e.g. cantilever wing), which assumes the occurrence of flutter in a lifting surface as unrelated to the rigid-body motion of the vehicle where it is mounted. Among the first studies on the interaction between aircraft motion and structural flexibility, the work presented in [2] which focused on high-speed forward swept wing aircraft, is foundational. The observed detrimental coupling between the rigid-body and the elastic dynamics of the vehicle, termed Body Freedom Flutter (BFF), was exemplified by means of a simple low-order model and a wealth of references where a similar problem had been investigated was provided. Recent studies [3–6] have confirmed, using more sophisticated models, that structural sizing aimed to achieve very light weight structure, and thus a significant degree of flexibility, could lead to multiple flutter mechanisms. Air vehicle layout, in terms of geometry and resulting aerodynamics, also plays a decisive role in the extent of this phenomenon. As a result, the aeroelastic sizing required to ensure flutter free behavior of the vehicle entails a multidisciplinary approach.

One of the contributions of the paper, which expands the initial work contained in [7], is to propose a simplified modeling process which, starting from the typical section model, attains a sufficiently sophisticated mathematical description of the system to capture some of the most relevant aspects of both the restrained wing flutter and the BFF. This framework is first employed to perform (a nominal parametric) flutter analysis of a representative wing-fuselage-tail flexible aircraft configuration where variations in two meaningful parameters are considered. The outcomes of this parametric analysis reveal interesting effects on flutter instability of modern aircraft design trends, such as lightweight structures and geometric layout with lower static stability.

However, another aspect further complicates the study of BFF. Despite the large amount of effort spent in understanding flutter, it is acknowledged that predictions based only on computational analyses are not totally reliable. One of the main reasons is the sensitivity of aeroelastic instabilities to small variations in parameter and modeling assumptions, as thoroughly reviewed in [8]. Currently, this is compensated by the addition of conservative safety margins to the analysis results as well as by expensive flutter tests campaigns. In addressing this difficulty, the so-called robust flutter analysis aims to quantify the gap between the prediction of the nominal stability analysis (model without uncertainties) and the worst case prediction when the whole set of uncertainty is contemplated. This method was first proposed for the study of flutter in [9, 10]. Other works that have addressed aeroelastic studies by means of robustness tools include: [11], which focused on model reduction, and [12] where different approaches for in-flight flutter analysis were investigated.

This study follows the approach of [9] in addressing this issue by making use of Linear Fractional Transformation (LFT) models and μ analysis [13, 14]- respectively, the modelling and analysis cornerstones of the so-called modern robust methods. The originality of this work is the methodological study of the potentialities of the LFT-μ paradigm for the study of the highly coupled dynamics of flexible aircraft exhibiting multiple instabilities. The interpretation of the results obtained within this framework requires an adequate familiarity with the tools underpinning the analyses; hence the paper first illustrates the manner in which robust techniques allow results found via conventional approaches (e.g. eigenvalue and graphical parametric sensitivity analysis) to be retrieved. Later, as the considered uncertain parameter space increases, the advantages in using robust techniques are critically discussed and the reconciliation of the findings with different physical aspects of the problem is described.

The paper show that the proposed robust approach to study flexible aircraft aeroelastic instabilities represents a powerful tool when used as a complement to the classical techniques. On the one hand, it provides a quantitative assessment of the system stability degradation in the face of uncertainties belonging to different fields (structural, aerodynamic, flight mechanics). In that regard, it could highlight weak points of the model requiring more refinement and conversely identify parameters that can be coarsely estimated as they do not have a strong influence on the results.

And on the other hand, the obtained results can be used to interpret the outcomes of standard parametric analyses, and the additional gained insight can be exploited in the definition of system properties during the conceptual design stage (when the availability of accurate and time-efficient modeling and analysis tools is paramount).

The layout of the article is as follows. Section II discusses the build up of the proposed BFF model which enables key features of this phenomenon to be captured. This model is built in a form amenable to application of LFT modeling techniques (required to efficiently recast the problem in the robust analysis framework). Section III presents the results obtained with the adopted model applying the p-k method, a classical algorithm for nominal flutter analyses. Section IV provides an introduction to the robustness tools employed in this work, and Section V finally shows the application of the LFT modeling process and μ analysis framework to the BFF problem and discusses the various results.

II. Aeroelastic model

In aircraft design, vehicle dynamics modeling and analysis are often addressed considering the rigid-body dynamics and the structural dynamics separately, on account of a wide frequency separation between the two sets of natural modes. However, this hypothesis is being challenged by the increased trend towards an optimal structural sizing and lightweight material selection, as well as by the conception of aircraft geometric layouts with low static stability (or statically unstable) but compensated with full-authority control systems. The enhanced coupling between the rigid and flexible dynamics thus compels consideration of a model retaining both aeroelastic and flight mechanics physical effects. In this Section the development of a simplified model to address this task is described. First, the typical section is introduced and it is shown to enable prediction of the instability of simple wing configurations (Subsection II A). Then, starting from the restrained wing model, a more comprehensive description is built up featuring also the rigid-body motion of the aircraft (Subsection II B).

A. Restrained wing model

The *typical section* model, see Fig. 1, was introduced in the early stages of aeroelasticity to investigate dynamic instabilities such as flutter [1]. Despite its simplicity, it captures the essential

effects of this phenomenon.

From the structural side, it basically consists of a rigid airfoil with lumped springs simulating the Degrees Of Freedom (DOFs) of the section, limited in this case to plunge h and pitch α. The positions of the elastic axis (EA), center of gravity (CG) and the aerodynamic center (AC) are also marked in Fig. 1. The main parameters in the model are: K_h and K_α (respectively the linear and rotational stiffness); half chord distance b; dimensionless distances a (from mid-chord to elastic axis) and x_α (from elastic axis to airfoil center of gravity). In addition to these parameters, the inertial characteristics of the system are given by: the mass ratio m_w (wing weight per unit span) and the moment of inertia of the section about the elastic axis I_α.

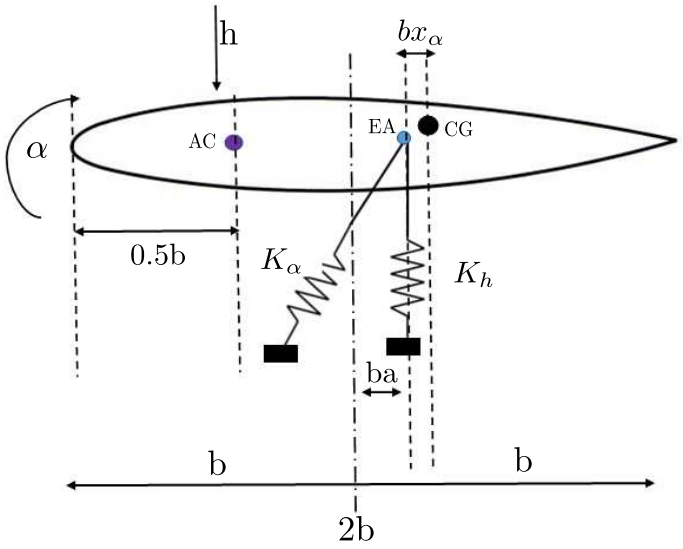

Fig. 1 Typical section sketch

For the modeling of the aerodynamic loads, the unsteady formulation proposed by Theodorsen [1] is employed. This approach is based on the assumption of a thin airfoil moving with small harmonic oscillations in a potential and incompressible flow.

In order to present the basic model development approach, the vectors $\mathbf{X}^E = [\frac{h(t)}{b}\ \alpha(t)]^T$ and $\mathbf{L_a}^E = [-L_h\ M_\alpha]^T$ are respectively defined for the elastic DOFs and the corresponding aerodynamic loads. The set of differential equations describing the dynamic equilibrium can then be recast in matrix form using Lagrange's equations [1]:

$$[\mathbf{M_s}]\ddot{\mathbf{X}}^E + [\mathbf{K_s}]\mathbf{X}^E = \mathbf{L_a}^E \tag{1}$$

where $\big[\mathbf{M_s}\big]$ and $\big[\mathbf{K_s}\big]$ are respectively the structural mass and stiffness matrices (structural damping is assumed null). They can be written as:

$$\big[\mathbf{M_s}\big] = m_w b \begin{bmatrix} 1 & x_\alpha \\ x_\alpha & r_\alpha^2 \end{bmatrix}; \qquad \big[\mathbf{K_s}\big] = \begin{bmatrix} bK_h & 0 \\ 0 & \frac{K_\alpha}{b} \end{bmatrix} \tag{2}$$

where $r_\alpha = \sqrt{\frac{I_\alpha}{m_w b^2}}$ is the dimensionless radius of gyration of the section about the elastic axis.

The Theodorsen model provides an expression of $\mathbf{L_a}^E$ in the Laplace s domain as:

$$\mathbf{L_a}^E(s) = q\big[\mathbf{A}(\bar{s})\big]\mathbf{X}^E(s) \tag{3}$$

where the dynamic pressure q, the dimensionless Laplace variable $\bar{s}$ ($=s\frac{b}{V}$ with V the airspeed) and the generalized Aerodynamic Influence Coefficient (AIC) matrix $\mathbf{A}(\bar{s})$ are introduced.

The final aeroelastic equilibrium is written in the frequency domain as:

$$\Big[\big[\mathbf{M_s}\big]s^2 + \big[\mathbf{K_s}\big] - q\big[\mathbf{A}(\bar{s})\big]\Big]\mathbf{X}^E(s) = \mathbf{0} \tag{4}$$

The premise of the typical section modeling is that the dynamics of an actual wing can be investigated choosing the aforementioned properties to match those at a span station about 70% distant from the aircraft centerline. Experience and studies (see references in [1]) have confirmed that this assumption is reasonable for wing configurations having large aspect ratio, small sweep angle and spanwise characteristics varying smoothly.

In order to specialize Eq. (4) to the study of uniform wings, the structural mass matrix $\mathbf{M_s}$ can be defined based on the inertial properties of the section at the proper wing station. As for the structural stiffness matrix $\mathbf{K_s}$, an equivalence in terms of the first *uncoupled* bending (ω_b) and torsional (ω_t) natural frequencies of a cantilever beam is imposed. First, structural properties commonly used to characterize the wing elasticity, such as bending stiffness EI and torsional stiffness GJ, are introduced. Then, two relations imposing the equivalence between the typical section and the uniform wing are written down in order to find the values for the typical section stiffness parameters K_h and K_α to be substituted in Eq. (2). The following holds [15]:

$$\begin{aligned} \omega_b &= \Big(0.597\frac{2\pi}{L}\Big)^2\sqrt{\frac{EI}{m_w}} = \sqrt{\frac{K_h}{m_w}} \\ \omega_t &= \frac{\pi}{L}\sqrt{\frac{GJ}{I_\alpha}} = \sqrt{\frac{K_\alpha}{I_\alpha}} \end{aligned} \tag{5}$$

The aerodynamic part of the system is the same as for the typical section, with the airfoil coefficients specialized to the geometry of the wing station. The 2D flow assumption is in line with the other hypotheses on the wing underlying this approach (which allow 3D effects to be neglected).

A prototype of a valid wing described by this model is shown in Fig. 2. The mean aerodynamic chord $\bar{c}$ and the span L are new parameters present in this problem.

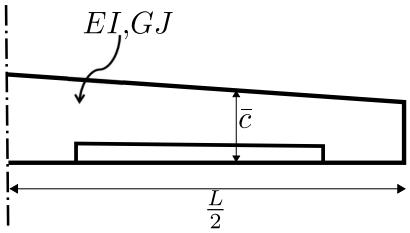

Fig. 2 Straight wing geometry

B. Flexible aircraft model

In order to extend the field of application of the analyses to the interactions of the wing flexibility with the motion of the aircraft, the previous model is augmented with rigid-body effects. Reference [16], which provides a comprehensive study on this subject, is taken as inspiration to outline a possible strategy.

The aircraft geometry considered is a wing-fuselage-tail configuration. The wing is assumed to be described by the model in Subsection IIA, while new parameters are introduced for the vehicle properties. Geometry parameters include the tail leading edge distance from the nose D, the tail span L_t and the mean chord c_t (S_t=$L_t c_t$ is the resulting tail surface). The inertia quantities considered are: tail (m_t) and wing (m_w) mass ratios, payload m_p, and total aircraft mass m; the vehicle pitch moment of inertia I_{yy} (similarly composed of payload pitch inertia I_{yy_P}, wing inertia I_{yy_w} and tail inertia I_{yy_t}). Aerodynamic properties such as wing and tail lift effectiveness coefficients $C^w_{L_\alpha}$ and $C^t_{L_\alpha}$ are also specified. A prototype of the air vehicle is sketched in Fig. 3.

Only the longitudinal dynamics are retained in the derived model, resulting in three additional states: the vehicle angle of attack $\bar{\alpha}$, the pitch angle $\bar{\theta}$ and its pitch rate $\bar{q}$. This is the *short period approximation*, which for conventional aircraft involves rapid heave and pitch oscillations at almost constant translational speed. Surge velocity is neglected since, as discussed in [6], the phugoid mode has a marginal role in the occurrence of the instability investigated here. The description of the

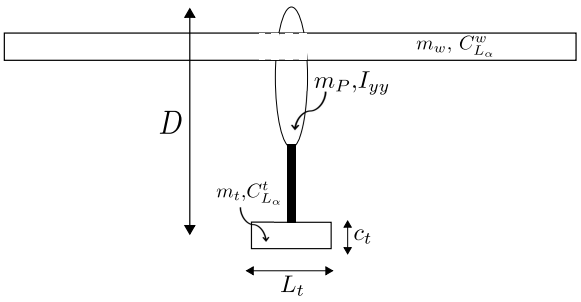

Fig. 3 Simplified aircraft geometry

longitudinal dynamics for level flight is given in the frequency domain by [16]:

$$\begin{bmatrix} (mV - Z_{\dot{\bar{\alpha}}})s - Z_{\bar{\alpha}} & -(Z_{\bar{q}} + mV)s \\ -(M_{\dot{\bar{\alpha}}}s + M_{\bar{\alpha}}) & I_{yy}s^2 - M_{\bar{q}}s \end{bmatrix} \begin{bmatrix} \bar{\alpha}(s) \\ \bar{\theta}(s) \end{bmatrix} = \begin{bmatrix} 0 \\ 0 \end{bmatrix} \tag{6}$$

where $\bar{q} = s\bar{\theta}$, $\mathbf{X}^R = [\bar{\alpha}\ \bar{\theta}]^T$ is the vector of rigid-body degrees of freedom, and the aerodynamic stability derivatives $Z_{\bar{\alpha}}$, $Z_{\dot{\bar{\alpha}}}$, $Z_{\bar{q}}$, $M_{\bar{\alpha}}$, $M_{\dot{\bar{\alpha}}}$, $M_{\bar{q}}$ have been introduced.

The characteristic equation associated with the system in Eq. (6) is a third order polynomial with one pole at the origin and the remaining second-order polynomial expressing the short-period approximation properties:

$$\begin{aligned} & s^2 + 2\zeta_{SP}\omega_{SP}s + \omega_{SP}^2 = 0 \\ & \omega_{SP}^2 \approx \frac{M_{\bar{q}}}{I_{yy}}\frac{Z_{\bar{\alpha}}}{mV - Z_{\dot{\bar{\alpha}}}} - \frac{M_{\bar{\alpha}}}{I_{yy}}\frac{mV + Z_{\bar{q}}}{mV - Z_{\dot{\bar{\alpha}}}} \\ & 2\zeta_{SP}\omega_{SP} \approx -(\frac{M_{\bar{q}}}{I_{yy}} + \frac{Z_{\bar{\alpha}}}{mV - Z_{\dot{\bar{\alpha}}}} + \frac{M_{\dot{\bar{\alpha}}}}{I_{yy}}\frac{mV + Z_{\bar{q}}}{mV - Z_{\dot{\bar{\alpha}}}}) \end{aligned} \tag{7}$$

All the aerodynamic stability derivatives are evaluated using a first-order approximation:

$$Z_\bullet = \frac{\partial Z}{\partial \bullet} = -qSC_{L_\bullet}; \qquad M_\bullet = \frac{\partial M}{\partial \bullet} = \bar{c}qSC_{M_\bullet}; \tag{8}$$

where $\bullet = \{\bar{\alpha}, \bar{q}, \dot{\bar{\alpha}}\}$ and $C_{L_\bullet}$, $C_{M_\bullet}$ are functions of the aircraft's geometry [16].

The final task is to determine the coupling terms, since the equilibrium of the elastic degrees of freedom has already been stated in Eq. (4). The crucial aspects to address are: the understanding of how the deformation affects the aerodynamic forces generated by the vehicle, and how the motion of the vehicle contributes to change the loads acting on the structure. A proposed simplification commonly accepted to study stability of flexible aircraft is to consider the fuselage and tail as rigid [17], which means that all the elasticity is concentrated in the wing.

First, the change in aerodynamic forces and moments produced by the aircraft due to the flexibility

is considered. The effect of the elastic deformation on the lift generated by the *local* wing sections is highlighted in the expression of the local angle of attack $\alpha_{loc} = \alpha_0 + \alpha + \frac{\dot{h}}{V}$, where α_0 is the rigid-body angle of attack of the section, related through the twist to $\bar{\alpha}$. The aeroelastic stability derivatives describing the effect of the deformation on the vehicle forces and moments can then be derived:

$$\begin{cases} C_L^w = C_L^{w,R} + C_L^{w,E} \\ C_L^w = C_{L_\alpha}^w(\alpha_0 + \alpha + \frac{\dot{h}}{V}) \end{cases} \Rightarrow \begin{array}{l} C_L^{w,R} = C_{L_\alpha}^w \alpha_0 \\ C_L^{w,E} = C_{L_\alpha}^w(\alpha + \dfrac{\dot{h}}{V}) \end{array} \tag{9}$$

where $C_{L_\alpha}^w$ is the wing lift effectiveness, $C_L^{w,R}$ is the rigid wing lift coefficient (accounted for in the aerodynamic derivatives previously introduced in Eq. (8)) and $C_L^{w,E}$ its elastic counterpart. This procedure leads to the definition of the *aeroelastic* stability derivatives Z_α and $Z_{\dot{h}}$, and follows the same line of reasoning to obtain M_α and $M_{\dot{h}}$ given the geometry of the wing and the relative position of center of gravity and aerodynamic centers. Note that for these coupling terms, describing the effect of wing deformation on the rigid equilibrium, the hypothesis of quasi-steadiness is assumed in order to keep consistency with the assumptions taken in evaluating the aerodynamic stability derivatives in Eq. (8).

Vehicle motion, by means of the rigid DOFs, in turn influences the loads acting on the wing. Specifically, a change in angle of attack $\bar{\alpha}$ and pitch rate $\bar{q}$ causes elastic terms containing $\frac{\dot{h}}{b}$ and α to generate further loads on the structure. If a quasi-steady flow is considered, then the procedure follows the one outlined in Eq. (9). More interestingly, when unsteadiness is retained, the relation between displacements and forces mimics the Theodorsen model introduced in Eq. (3). In particular, it is possible to write in the Laplace domain:

$$\mathbf{L_a}^R(s) = q\big[\mathbf{A}\big]\big[\mathbf{T}\big]\mathbf{X}^R(s) \tag{10}$$

where $\big[\mathbf{T}\big]$ is a transformation matrix allowing the typical section degrees of freedom $\mathbf{X}^E$ in terms of $\mathbf{X}^R$ to be expressed. This defines the remaining aeroelastic stability derivatives $L_{\bar{\alpha}}$, $L_{\bar{q}}$, $M_{\bar{\alpha}}$, $M_{\bar{q}}$.

A short-hand expression for the full system is given by:

$$\left[s^2 \begin{bmatrix} \boldsymbol{M_{RR}} & \boldsymbol{M_{RE}} \\ \boldsymbol{M_{ER}} & \boldsymbol{M_{EE}} \end{bmatrix} + s \begin{bmatrix} \boldsymbol{C_{RR}} & \boldsymbol{C_{RE}} \\ \boldsymbol{C_{ER}} & \boldsymbol{C_{EE}} \end{bmatrix} + \begin{bmatrix} \boldsymbol{K_{RR}} & \boldsymbol{K_{RE}} \\ \boldsymbol{K_{ER}}(\bar{s}) & \boldsymbol{K_{EE}}(\bar{s}) \end{bmatrix} \right] \begin{bmatrix} \mathbf{X}^R \\ \mathbf{X}^E \end{bmatrix} = \begin{bmatrix} \mathbf{0} \\ \mathbf{0} \end{bmatrix} \tag{11}$$

where the subscripts $\boldsymbol{R}$ and $\boldsymbol{E}$ refer again to the Rigid-body and Elastic DOFs. Note that if the cross-coupling terms ($\boldsymbol{RE}$ or $\boldsymbol{ER}$) are set to zero, the study of the dynamics of the system amounts to separate consideration of the short-period approximation of the aircraft (governed by the $\boldsymbol{RR}$ terms) and the restrained wing aeroelastic problem (described by the $\boldsymbol{EE}$ terms).

In Eq. (11) relevant aspects of the rigid-elastic coupling are featured. The aeroelastic derivatives calculation process, outlined in Eqs. (9)-(10), follows the modeling construct rationale of [16], despite the significant simplifications adopted in this model. It is also noted that BFF is well predicted using linear models for the aircraft and is not the result of aerodynamic or structural nonlinearities [3], hence the hypotheses underpinning the dynamics in Eq. (11).

The goal of the presented mathematical model is twofold: on the one side, to retain important features of the interaction between elastic and rigid modes (this aspect will be fully explored in Section III); and on the other hand, to provide a manageable starting point for the definition of reliable LFT models (this instrumental step in the investigation of the robustness of the system will be addressed in Subsection V A).

III. Nominal analysis

Nominal flutter analysis studies the conditions at which the dynamic aeroelastic system, at a fixed, known condition, loses its stability. This is a parameter-dependent problem, since as a parameter of the model is varied, the system's behavior changes. Generally, this is accomplished considering the air stream *speed* V as the critical parameter, and the result is the definition of a speed V_f, called flutter speed, such that for all the speeds below it the system is stable.

Subsection III A presents the restrained wing flutter analyses performed on the general model from Subsection II A, and validating it with the Goland wing benchmark. Subsection III B showcases and discusses the results obtained analyzing a notional flexible aircraft configuration. The values of the parameters defining the test case are given in Appendix in Table 4. Their selection is discussed in Subsection III B.

A. Restrained wing model validation

The capability of the model built in Subsection II A in predicting flutter onset of simple wing geometries is validated against the Goland wing, a well-known benchmark problem in the literature [18]. This benchmark consists of a uniform rectangular wing with constant structural and

inertial properties along the span and no control surfaces. This last feature can be seen as the consequence of the natural frequency associated with this mode being much greater than the ones related to bending and torsion modes.

The numerical algorithm employed in this work to perform nominal flutter analyses is the p-k method [19]. This algorithm, a standard method for flutter analysis, is a natural choice due to the frequency domain formulation of the problem (recall Eq. (11)). Fig. 4 displays the results of the analyses. In Fig. 4(a) the eigenvalues corresponding to the two elastic modes are depicted as the airstream speed is increased (the first speed analyzed is identified in the figure with square markers). At a speed V_f=141 $\frac{m}{s}$ (denoted by circle markers) the system exhibits an instability dominated by the torsion mode. Note that ω_f=73.2 $\frac{rad}{s}$ refers to the flutter frequency (i.e. the frequency of the torsion mode at flutter), while ω_{b-f}=63.1 $\frac{rad}{s}$ refers to the frequency of the bending mode at V_f. The evolution of the mode frequencies as speed increases is shown in Fig. 4(b), with the dotted vertical line emphasizing the flutter point.

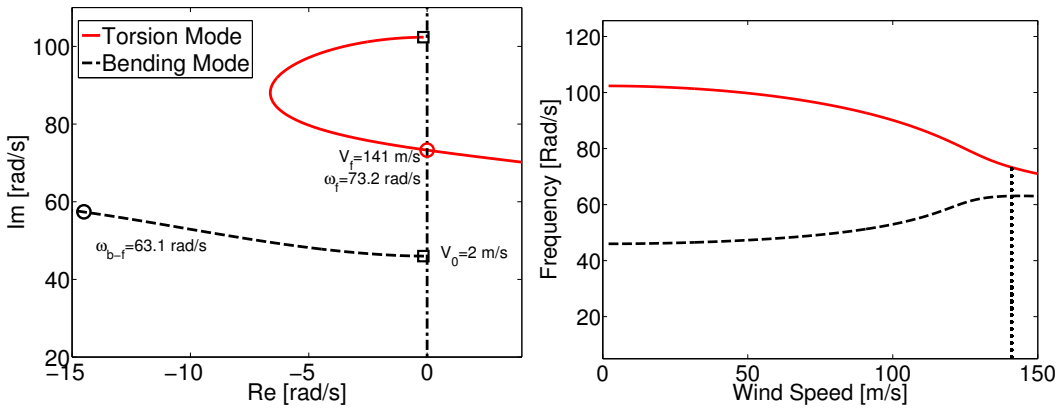

(a) Poles variation

(b) Frequency variation

Fig. 4 Goland wing benchmark: bending and torsion modes variation with speed

In Table III A a comparison of the results obtained in this work with others from the literature is shown. There is a satisfactory matching with another 2D approximation of the straight wing model [20], while the discrepancies with an aeroelastic model comprising 3D effects [18] remain below 3% in terms of V_f. In this regard, it is remarked here that, although the aspect ratio of the Goland wing is not considered to be high, the model proposed in Sec. II is still able to adequately capture its flutter behaviour. This can be ascribed to the simple geometry of the wing (null sweep

angle, uniform geometrical properties) which reduces 3D aerodynamic effects.

Table 1 Comparison of results for the Goland wing flutter analysis

	Flutter velocity $[\frac{m}{s}]$	Flutter frequency $[\frac{rad}{s}]$
Present work	141.1	73.2
2D approximation [20]	141.2	72.5
Original reference [18]	137.2	70.7

B. Study of flexible aircraft instabilities

The analysis shown in Subsection III A gives a prediction about instability occurrence considering the wing by itself (i.e. *restrained* model). This implies assuming flutter onset as unrelated to the rigid-body motion of the vehicle on which the aerodynamic body is mounted. In Section II the reasons to contemplate a more sophisticated model (including the vehicle motion and its coupling with the wing elasticity) were motivated. The model built up therein enables studies on the so-called Body Freedom Flutter (BFF) to be performed, which are presented and discussed next.

1. Preliminary considerations and test case definition

The aircraft geometry considered in this work was depicted in Fig. 3. It is remarked here that the pursued analyses are not aimed at investigating the stability of a specific air vehicle layout. Instead, the chief goal is to show how the proposed (simplified) aircraft model incorporates features of BFF.

Different studies on this topic [5, 17, 21, 22] highlighted common design features which are responsible for amplifying the interaction between rigid and elastic dynamics. These references showed that inertia and stiffness play a decisive role in modifying free-vibration properties, bringing the lowest elastic natural frequencies closer to the frequencies characteristic of the vehicle motion. They also modify the corresponding mode shapes [3]. Similarly, aircraft geometry (with its associated effect on the stability derivatives) is also decisive. An example of this is represented by the tail volume V_H parameter, which as shown in [22] can exacerbate the interaction between the rigid-body short period and the wing first bending mode when of low value. This parameter is defined as

$$V_H = (\bar{X}^t_{AC} - \bar{X}_{CG})\frac{S_t}{S} \tag{12}$$

where $\bar{X}^t_{AC}$ and $\bar{X}_{CG}$ are respectively the dimensionless (dividing by the mean aerodynamic chord $\bar{c}$) distances from the aircraft nose to respectively, the tail aerodynamic center and the aircraft center of gravity. Once the lifting surfaces' sizes and inertial properties are fixed, V_H is a function of D (the distance from the nose to the tail leading edge), which was introduced in Subsection II B and also explicitly depicted in Fig. 3. This parameter directly influences the value of $\bar{X}^t_{AC}$ which is known to have great effect on the aerodynamic stability derivatives of Eq. (8).

The above considerations inform the selection of the parameters defining the vehicle configuration. The wing is described by the same parameters that define the Goland wing, with the only exception of EI, which in here is assumed to represent an *aeroelastic* design variable that reflects the tendency towards a lightweight-oriented structural sizing. This design variable is given by $EI{=}\sigma_s EI_G$ with EI_G set at the value for the Goland wing and σ_s, referred to as the *bending stiffness factor*, ranging within prescribed values. Thus, EI represents a free parameter capturing the range of bending stiffness and taking values from maximum bending flexibility (σ_s=0.05) to maximum bending rigidity (σ_s=1).

Note that the wing mass ratio m_w is kept constant at the Goland wing value, although it could be argued that the chosen variation in bending stiffness implies also a variation in weight. This assumption is dictated by the aim at this stage to investigate how the proposed model captures the effect on BFF of specific parameters related to aeroelastic and flight mechanics design aspects. Torsional stiffness is also kept constant because, as shown in Fig. 4(a), this mode is dominating the flutter behavior of the wing and thus a design constraint in terms of its lower value is assumed to hold.

With respect to the flexible aircraft layout, the parameters defining the geometrical and inertial properties are obtained by scaling the values from [17] (which examines a similar aircraft layout) through adopting the Goland wing mass ratio and span as the reference mass and length. As an example, the definition of the vehicle payload pitch inertia I_{yy_P} becomes:

$$I_{yy_P} = I^0_{yy_P}\left(\frac{m_w}{m^0_w}\right)\left(\frac{L}{L^0}\right)^2 \tag{13}$$

where the variables with superscript 0 represent the values from [17]. Finally, the other design parameter used is the position of the tail D, which represents the *flight mechanics* design variable,

due to its important role discussed earlier. This parameter is assumed to vary in a range between 5 m and 10 m, complying with static stability requirements.

2. Results

Following a traditional parametric analysis approach, Fig. 5 shows the flutter speed V_f, i.e. the lowest speed at which the system loses stability, considering a grid of values for the design parameters EI and D. Three values of the bending stiffness factor σ_s (marked by vertical dashed lines) are highlighted and will be discussed subsequently.

The first apparent feature observed in Fig. 5, and very familiar to aeroelasticians [1], is that the tendency for instability is more pronounced as the bending ω_b and torsional ω_t frequencies become closer. This is seen by the slope of the restrained wing (solid line), where it is evident that V_f increases as σ_s (equivalently EI) is reduced. This is due to the fact that a decrease in EI implies an analogous trend in the bending frequency, as expressed by Eq. (5). Since the torsional stiffness is kept constant in these analyses, a decrease in σ_s can hence be interpreted as a reduction in the ratio $\frac{\omega_b}{\omega_t}$ between the uncoupled bending and torsional natural frequencies.

The flutter velocities obtained when rigid-elastic interactions are included (curves for D={5,6,8,10} m in Fig. 5) maintain the above trend but only for as long as the tail volume of the vehicle does not become critical to the stability. In fact, there is a whole range of bending flexibility values of the wing ($0.15<\sigma_s<1$) where V_H proves to have a negligible influence on flutter occurrence, and thus the BFF model predicts only a relatively small decrease in flutter speed with respect to the restrained model (up to 3%). But as the bending flexibility increases ($\sigma_s<0.15$), the interaction between the short-period and the bending mode becomes significant, which leads to an abrupt decrease of flutter speed. Therefore, tail volume is confirmed to play a crucial twofold role: it prompts rigid-elastic coupling (in that it changes the σ_s threshold at which the leap occurs) and it determines the magnitude of the change in the V_f value itself. In particular, Fig. 5 shows that a lower D (i.e. lower V_H) anticipates the transition to the BFF mechanism and determines a lower flutter speed than for the scenario with greater V_H, confirming its role discussed earlier.

The behaviour detected in Fig. 5 can be better clarified observing the trend of the eigenvalues, see Fig. 6, for two aircraft configurations. Tail distance D is for both cases equal to 5 m, while the

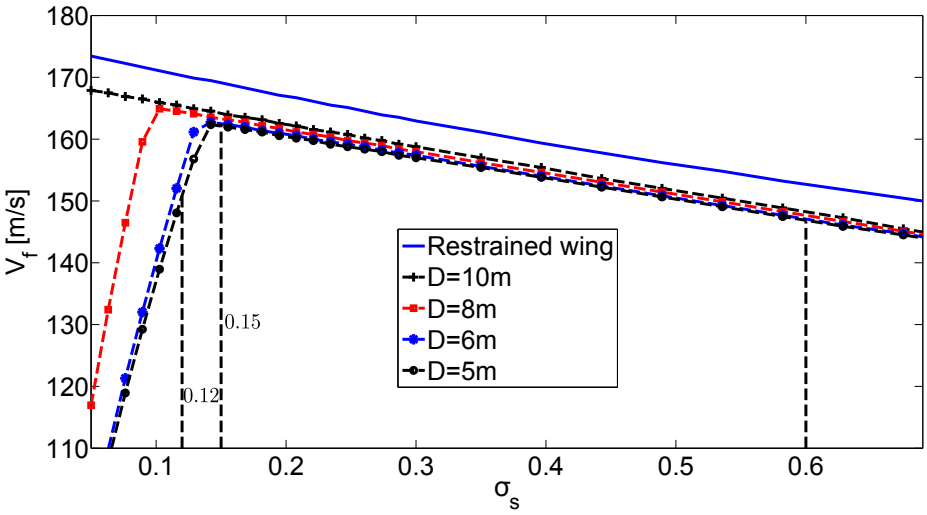

Fig. 5 Flutter speed of the flexible aircraft at a grid of EI (i.e. σ_s) and D values.

bending stiffness parameter σ_s is equal to 0.6 for case A and to 0.12 for case B (these cases are two of those highlighted in Fig. 5 with vertical dashed lines). Hence they each belong to one of the two *stability regions* detected in the plot.

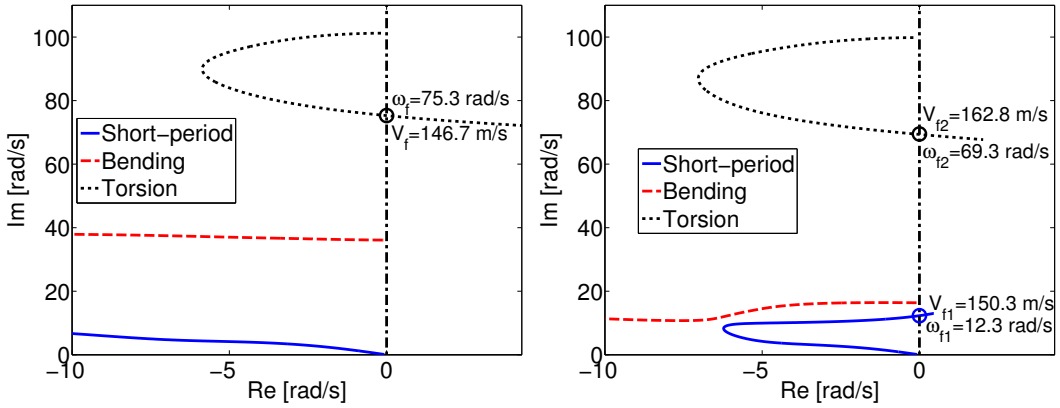

(a) Case A: torsional-bending instability

(b) Case B: BFF instability

Fig. 6 Eigenvalues location as a function of speed within BFF model

In Fig. 6 the modes branches are identified (and labeled) according to their genesis of pure rigid-body or pure elastic modes. However, it is fair to remark that all the modes experience coupling due to the aerodynamics (*bending* and *torsion*) and to motion (*short period* and *bending*), and hence this labeling is only a naming convention for ease of explanation. For the first aircraft configuration, depicted in Fig. 6(a), the eigenvalues of the system exhibit a pattern qualitatively similar to the one shown in Fig. 4(a) for the (restrained) Goland wing model. In fact, the flutter mechanism does not involve coupling with rigid motion and it is the torsional mode which goes unstable at V_f=146.7

$\frac{m}{s}$ and ω_f=75.3 $\frac{rad}{s}$ (high frequency instability). The short-period eigenvalue follows the pattern known for the pure rigid-body case (with a frequency increasing almost linearly with speed), and thus proves to be almost unperturbed by the wing deformation. However, when bending flexibility becomes more prominent (i.e. case B shown in Fig. 6(b)) two distinctive flutter mechanisms can be observed. The first imaginary axis crossing takes place at a speed V_{f1}=150.3 $\frac{m}{s}$ and at a frequency ω_{f1}=12.3$\frac{rad}{s}$. This low-frequency instability is the result of the interaction between the short-period and the bending modes (that is, the Body Freedom Flutter). The second crossing takes place at V_{f2}=162.8 $\frac{m}{s}$ at a higher frequency (ω_{f2}=69.3$\frac{rad}{s}$), and is dominated by the torsion instability already encountered in the other configuration.

In conclusion, the trend depicted in Fig. 5 is motivated by a change in the mode first reaching the flutter condition, which for the curves D={5,6,8} m (in the range of low bending stiffness, i.e. the left side of Fig. 5) is the rigid-elastic coupled mode, while in the other cases is still the torsional mode (as clearly demonstrated in Fig. 6).

As a prelude to the following section, and serving as a summary of this one, it is noted that:

- The above results confirm that the proposed model from Section II is able to capture known physical effects of the BFF problem.

- The use of standard methods (e.g. *p-k*) for flutter sensitivity analysis can show the detrimental effect on stability for the BFF problem (Fig. 5) and provides a characterization of the multiple instabilities affecting the system by tracking the eigenvalues of the system as the airspeed is varied (Fig. 6). The procedure implies a gridding of the parameter space and therefore it does not provide theoretical guarantees on the results.

- Due to the latter gridding, when dealing with a larger number of variables, a parametric study such as the one performed in this subsection is expected to become difficult to interpret and computationally onerous. As the sizing required to ensure a flutter free behavior of flexible aircraft is inherently multidisciplinary, the opportunity to propose an approach, built on a robustness modeling and analysis framework, which attempts to overcome the aforementioned issues is envisaged.

IV. Theoretical Background

This Section provides a cursory introduction to LFT [13] and μ analysis [14]. The interested reader is referred to the aforementioned references for a thorough overview of these techniques. They have been applied in the last two decades to the study of complex uncertain systems in the aerospace field: see for example [23] for LFT modeling and [24] for μ and related worst-case analysis. Further, in [25] their application to the structural and control optimization problem of an aeroservoelastic system was presented.

A. Linear Fractional Transformation

LFT is an instrumental framework in modern control theory for robustness analysis and synthesis. The underpinning idea is to represent an uncertain system in terms of nominal and uncertain components given by matrices.

Let $\mathbf{M} \in \mathbb{C}^{(p_1+p_2)\times(q_1+q_2)}$ be a matrix partitioned as $\mathbf{M} = [\mathbf{M_{11}}\ \mathbf{M_{12}};\ \mathbf{M_{21}}\ \mathbf{M_{22}}]$ and $\mathbf{\Delta_u} \in \mathbb{C}^{q_1\times p_1}$. The upper LFT with respect to $\mathbf{\Delta_u}$ is defined as the map:

$$\begin{aligned} &\mathcal{F}_u(\mathbf{M}, \bullet) : \mathbb{C}^{q_1\times p_1} \longrightarrow \mathbb{C}^{p_2\times q_2} \\ &\mathcal{F}_u(\mathbf{M}, \mathbf{\Delta_u}) = \mathbf{M_{22}} + \mathbf{M_{21}}\mathbf{\Delta_u}(\mathbf{I} - \mathbf{M_{11}}\mathbf{\Delta_u})^{-1}\mathbf{M_{12}} \end{aligned} \tag{14}$$

Fig. 7 shows the feedback representation usually adopted to depict $\mathcal{F}_u(\mathbf{M}, \mathbf{\Delta_u})$ (the subscript in $\mathbf{\Delta_u}$ will be dropped in the following). If $\mathbf{M}$ is taken as a proper transfer matrix, $\mathcal{F}_u$ is the closed-loop transfer matrix from input $\mathbf{u}$ to output $\mathbf{y}$ when the nominal *plant* (i.e. the system with no uncertainty) $\mathbf{M_{22}}$ is subject to a perturbation matrix $\mathbf{\Delta}$. A crucial feature apparent in Eq. (14) is that the LFT is well posed if and only if the inverse of $(\mathbf{I} - \mathbf{M_{11}}\mathbf{\Delta})$ exists, where $\mathbf{M_{11}}$ is by definition the transfer matrix seen by the perturbation block $\mathbf{\Delta}$.

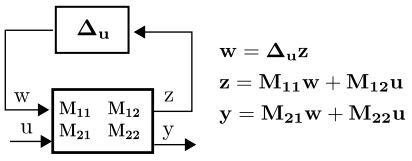

Fig. 7 Upper Linear Fractional Transformation (LFT).

B. μ analysis

μ, also known as structured singular value (s.s.v.) analysis, enables the robust stability and performance of a system subject to real parametric and dynamic uncertainties to be addressed.

The s.s.v. is a matrix function denoted by $\mu_{\mathbf{\Delta}}(\mathbf{M_{11}})$:

$$\mu_{\mathbf{\Delta}}(\mathbf{M_{11}}) = \left(\min_{\hat{\mathbf{\Delta}} \in \mathbf{\Delta}} (\beta : \det(\mathbf{I} - \beta \mathbf{M_{11}} \hat{\mathbf{\Delta}}) = 0; \quad \bar{\sigma}(\hat{\mathbf{\Delta}}) \leq 1) \right)^{-1} \tag{15}$$

where β is a real positive scalar and $\mathbf{\Delta}$ is the structured uncertainty set associated with $\mathcal{F}_u(\mathbf{M}, \mathbf{\Delta})$. For ease of calculation and interpretation, and without loss of generality, this set is norm-bounded (i.e. $\bar{\sigma}(\mathbf{\Delta}) \leq 1$) by scaling of $\mathbf{M_{11}}$. The result can then be interpreted as a robust stability (RS) test of the plant represented by $\mathcal{F}_u(\mathbf{M}, \mathbf{\Delta})$: if $\mu_{\mathbf{\Delta}}(\mathbf{M_{11}}) \leq 1$ then there is no perturbation matrix inside the allowable set $\mathbf{\Delta}$ such that the determinant condition is satisfied. That is, $\mathcal{F}_u(\mathbf{M}, \mathbf{\Delta})$ is well posed and thus the associated plant is robustly stable within the range of uncertainties considered. On the contrary, if $\mu_{\mathbf{\Delta}}(\mathbf{M_{11}}) \geq 1$ a candidate (i.e. belonging to the allowed set) perturbation matrix exists which violates the well-posedness, i.e. the closed loop in Fig. 7 is unstable.

It is known that $\mu_{\mathbf{\Delta}}(\mathbf{M})$ is in general an NP-hard problem [13], thus all μ algorithms work by searching for upper (UB) and lower (LB) bounds. The upper bound μ_{UB} provides the maximum size perturbation $\bar{\sigma}(\mathbf{\Delta}_{UB}) = 1/\mu_{UB}$ for which RS is guaranteed, whereas the lower bound μ_{LB} defines a minimum size perturbation $\bar{\sigma}(\mathbf{\Delta}_{LB}) = 1/\mu_{LB}$ for which RS is guaranteed to be violated. If the bounds are close in magnitude then the conservativeness in the calculation of μ is small, otherwise nothing can be said on the guaranteed robustness of the system for perturbations within $[1/\mu_{UB}, 1/\mu_{LB}]$. A study on the performance and analysis effects of various μ algorithms was performed in [26] using specific flutter-related uncertainty descriptions. These tests suggested that the currently available algorithms are able to cope with the pure real problems of medium size that frequently arise in flutter analysis. It is crucial, however, in order to provide reliable predictions, to adopt the more appropriate algorithms among the options currently available. In this work, based on the outcome of the aforementioned study, the Balanced form algorithm is employed for μ_{UB} calculation, whereas the gain-based one [27] is adopted for μ_{LB}.

V. Robust analysis

This section exploits the capabilities of the robust modeling and analysis techniques presented in Section IV to further investigate the dynamic aeroelastic instabilities exhibited by simplified flexible aircraft configurations. The first subsection describes the LFT models employed in the analyses, followed by the presentation and discussion of the results.

A. LFT models

The goal of the LFT modeling process is to recast the aeroelastic system, described for the nominal case by Eq. (11), in the framework of Fig. 7 and Eq. (14). A systematic review of possible strategies to perform this task for aeroelastic applications is documented in [26], which contains a detailed study of the different problem formulations and uncertainty description options. In this work, the method outlined in [9], known as μ-k method, is adopted and the basic steps are recalled here.

First note that parametric uncertainties can be used to describe parameters whose values are varying or not known with a satisfactory level of confidence. Considering a generic uncertain parameter g, with λ_g indicating the uncertainty level with respect to a nominal value g_0 and $\delta_g \in [-1, 1]$ representing the uncertainty flag, a general uncertain representation is given by:

$$g = g_0 + \lambda_g \delta_g \tag{16}$$

This expression is often referred to as *additive* uncertainty [13]. At a matrix level, the operator $\mathbf{G}$ affected by parametric uncertainties can be expressed as:

$$[\mathbf{G}] = [\mathbf{G_0}] + [\mathbf{V_G}][\mathbf{\Delta_G}][\mathbf{W_G}] \tag{17}$$

where $\mathbf{V_G}$ and $\mathbf{W_G}$ are scaling matrices which, provided the uncertainty level λ_g for each parameter, give a structured perturbation matrix $\mathbf{\Delta_G}$ belonging to the norm bounded subset, i.e. $\bar{\sigma}(\mathbf{\Delta_G}) \leq 1$. These uncertainty blocks can be obtained by writing the uncertainty parameters in symbolic form and using, for instance, the well consolidated LFR toolbox [28] or alternative algorithms [29].

The first step is thus to use the additive uncertainty definition for the operators in Eq. (11) that are considered uncertain. The matrix uncertainty description obtained by applying Eq. (17) to the *aeroelastic stiffness* operator $\boldsymbol{K_{EE}}$ and the *rigid stiffness* operator $\boldsymbol{K_{RR}}$ is:

$$\begin{aligned} [\boldsymbol{K_{EE}}] &= [\boldsymbol{K_{EE}}^0] + [\mathbf{V_{K_{EE}}}][\mathbf{\Delta_{K_{EE}}}][\mathbf{W_{K_{EE}}}] \\ [\boldsymbol{K_{RR}}] &= [\boldsymbol{K_{RR}}^0] + [\mathbf{V_{K_{RR}}}][\mathbf{\Delta_{K_{RR}}}][\mathbf{W_{K_{RR}}}] \end{aligned} \tag{18}$$

In this example, uncertainties are assumed to affect the structural stiffness and the unsteady aerodynamic properties for the first operator (recall from Eq. (4) that $\boldsymbol{K_{EE}} = \mathbf{K_s} - q\mathbf{A}$), whereas variability of stability derivatives as $Z_{\bar{\alpha}}$ and $M_{\bar{\alpha}}$ are captured in $\boldsymbol{K_{RR}}$ (see the short period approximation in Eq. (6)). In general, this operation will provide for each considered operator the

auxiliary matrices $\mathbf{\Delta_\bullet}$, $\mathbf{V_\bullet}$, and $\mathbf{W_\bullet}$ (with $\bullet = \{\boldsymbol{M_\star}, \boldsymbol{C_\star}, \boldsymbol{K_\star}\}$ and $\star = \{\boldsymbol{RR}, \boldsymbol{RE}, \boldsymbol{ER}, \boldsymbol{EE}\}$).
Once this is accomplished, the uncertainty operators are substituted in Eq. (11) and the nominal dynamics is separated from the uncertain terms, leading to the evaluation of $\mathbf{M_{11}}$ which is the matrix used by μ analysis to perform the RS test (Eq. (15)).

This subsection is concluded with the definition of the LFTs employed in the subsequent analyses. Based on the discussions and evidence of the previous subsections, three important design variables are selected as the considered uncertainty parameters: wing bending stiffness EI, tail distance D, and wing mass ratio m_w.
The first two parameters and their role in the instabilities that the aircraft may encounter were amply commented on in Subsection III B 2. The wing mass is also a fundamental parameter of the flexible aircraft dynamics, since it significantly influences the rigid-body equilibrium: it alters the vehicle inertia properties (assumed to scale with the wing weight, as shown in Eq. (13) for the pitch inertia) as well as the CG location (with important effects on the short-period properties). In addition, the restrained wing flutter itself is known to be highly dependent on the inertial contribution and thus an uncertainty affecting the structural mass matrix (as m_w does, see definition of $\mathbf{M_s}$ in Eq. (2)) has substantial repercussions.
The reason to capture these parameters in an LFT fashion is therefore twofold. On the one hand, their values (especially EI and m_w) are only known within a certain tolerance until the final design stage and therefore all flutter analyses should take into account this uncertainty. On the other hand, they are key design variables selected during the conceptual design stage, typically characterized by different concurrent requirements, and hence additional insights are invaluable at that stage. For these reasons, it is of interest to explore the capabilities of μ in this highly coupled scenario.
In addition to these three parameters, uncertainty in some of the aerodynamic transfer functions (the generic terms A_{ij}) is considered to allow for inaccuracies in the aerodynamic model and potential violations in its underlying hypotheses (e.g. the fact that 3D effects are not necessarily negligible).

As aforementioned, an LFT model is formed by a nominal system and an associated uncertainty block $\mathbf{\Delta}$. For the latter, two uncertainty descriptions are adopted in this work, yielding 2 different

LFT models. Their schematic $\mathbf{\Delta}$ block representations are:

$$\begin{aligned}\mathbf{\Delta_1}^{8,R-3,C} &= \mathrm{diag}(\delta_D I_7, \delta_{EI}, \delta_{A_{12}}, \delta_{A_{21}}, \delta_{A_{22}}) \\ \mathbf{\Delta_2}^{18,R-3,C} &= \mathrm{diag}(\delta_{m_w} I_{10}, \delta_D I_7, \delta_{EI}, \delta_{A_{12}}, \delta_{A_{21}}, \delta_{A_{22}})\end{aligned} \tag{19}$$

where the size of the uncertainties (total $\mathbf{\Delta}$ dimension) and their nature (real R or complex C) is recalled in the superscripts, while I_n indicates the identity matrix of size n (for repeated uncertainties). These two LFTs both capture the variability in aerodynamics, bending stiffness, and tail distance, and for the second (LFT-2) also that for the mass ratio δ_{m_w}. Thus, LFT-1 will allow similar analyses to those from the previous section to be explored. Note that LFT-1 can be obtained as a particular realization of LFT-2 ($\delta_{m_w} = 0$). The uncertainty description for all the parameters reflect the additive relation given in Eq. (16). The aerodynamic uncertainties are complex and their uncertain description is such that they range in the disc of the complex plane centered in the nominal value and having a radius equal to 3% [26].

For μ analyses, an LFT model requires a stable, so-called *LFT nominal*, plant that is obtained by setting $\mathbf{\Delta}$ to zero. Both of the above LFT models are centered at $EI = 0.15EI_G$ (i.e. $\sigma_s = 0.15$, marked with a vertical dashed line in Fig. 5) and $D = 6$m. Using these values and m_w as in Table 4, the flutter speed of the corresponding aeroelastic system can be read off from Fig. 5 as $V_f = 162$ $\frac{m}{s}$. Therefore, the LFT nominal plant is centered at the sub-critical speed $V = 150$ $\frac{m}{s}$.

With reference to Fig. 5, it is worth noticing that the system is located close to the boundary between the two regions discussed in Subsection III B 2. In particular, this configuration features (for the specified value of tail distance) one of the highest flutter speeds, lying at the same time close to the abrupt leap in the flutter curve. From a flutter design perspective, this layout can thus be regarded as optimal in that it attains the highest flutter speed given a prescribed margin from BFF occurrence. It is therefore of interest to perform a thorough investigation looking at its robustness. In order to further characterize the flutter behaviour of this configuration, Fig. 8 shows the pole locations of the LFT nominal system, highlighting speeds and frequencies for the instabilities taking place. The system exhibits both the low frequency (Body Freedom Flutter at ω_1) and high frequency (restrained wing flutter at ω_2) instabilities. Note that in comparison to Fig. 6(b), the restrained wing flutter is the first to be encountered (i.e. corresponding to the lowest speed) at $V_{f2} = 162$ $\frac{m}{s}$

and $\omega_{f2} = 69.7\ \frac{rad}{s}$, while the BFF occurs at a speed $V_{f1} = 175\ \frac{m}{s}$ and a frequency $\omega_{f1} = 14.7\ \frac{rad}{s}$.

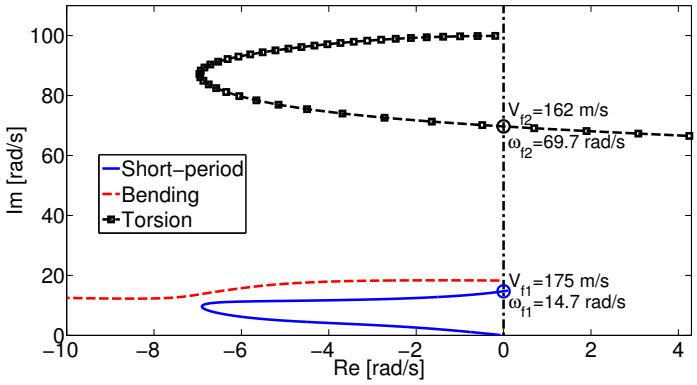

Fig. 8 Poles location as a function of speed for the nominal aircraft

B. μ-analysis results for LFT Model 1

Parametric sensitivity study. The first goal in using LFT-1 is to show the capability of μ analysis in inferring similar conclusions about the system's instabilities as those drawn in Subsection III B 2 via the manual parametric study. This is done here by assessing the role played by each uncertainty in the robust stability calculation, i.e. a type of robust parametric sensitivity analysis performed within the μ analysis framework. Once a condition is defined (for RS this is the determinant condition in Eq. (15) such that the LFT is ill-posed), μ highlights the relevance of the selected uncertainty parameter in the uncertainty block. Although more advanced μ sensitivity analyses can be employed using the skew-μ concept [30], this task is assessed here considering two different uncertainty levels (10% and 30%) for both the wing bending and the tail distance. Fig. 9 shows the μ results for the four different combinations of the two uncertainty ranges. Since the upper and lower bounds are close in each case, only the upper bounds are plotted for clarity. Before discussing the μ analyses of Fig. 9, the significance of the four range cases (RC1-#) is discussed based on the analyses of Fig. 5:

- RC1-A & RC1-B: the plant is expected to be robustly stable because when σ_s varies within 10% of its nominal value ($0.135 < \sigma_s < 0.165$) the flutter speed is always above 150 $\frac{m}{s}$;
- RC1-C & RC1-D: BFF is expected to occur at lower speeds than 150 $\frac{m}{s}$ because the rigid-elastic coupling could be magnified for certain allowed combinations of σ_s and D.

All the analyses show two distinctive peaks in the μ plot, a low frequency-one ω_1 at about $10\frac{rad}{s}$

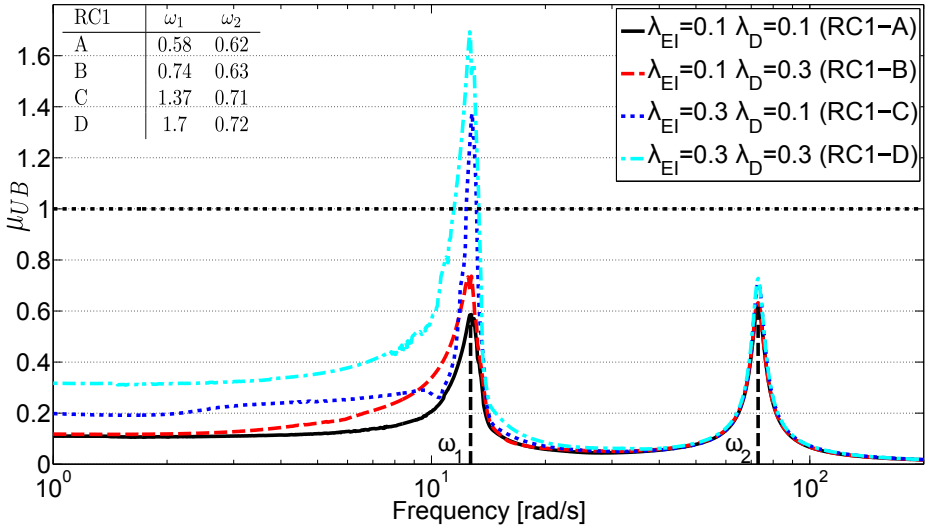

Fig. 9 μ analysis LFT-1: μ_{UB} sensitivity for different ranges (λ_{EI}, λ_D) of EI and D.

(related to the BFF mechanism) and a high frequency-one ω_2 at about $70\frac{rad}{s}$ (related to the torsion-bending coupling). The values of these peaks for each case are also highlighted in a dedicated table inset in Fig. 9. When the first uncertainty level RC1-A is considered (solid line), μ is smaller than 1 for the whole frequency range, indicating that the system is robustly stable in the face of the allowed uncertainties. The values of the peaks are respectively 0.58 at ω_1 and 0.62 at ω_2. When the tail distance uncertainty level is tripled in RC1-B (red dashed line), there is a greater increase in the low frequency peak (0.74) than in the high-one (0.63). This suggests that the BFF instability is more sensitive to variations on this parameter. When the wing bending stiffness is tripled in RC1-C (blue dotted line), the system RS undergoes a remarkable degradation. In particular the low frequency peak (1.37) is highly affected indicating that with the present uncertainty level the stability of the system is violated for the selected sub-critical speed of 150 $\frac{m}{s}$. Note that the predicted instability (i.e. the lower frequency) is the one that was deemed less critical according to the nominal analyses in Fig. 8. Finally, the scenario when both the parameters vary with a triple uncertainty level in RC1-D (cyan dash-dot line) results in an even more critical robustness degradation for the BFF (1.7), whereas the high frequency instability is almost unchanged (0.72).

Stability-based results in support of system level decisions. For an easier interpretation of these results, Fig. 5 and the related comments should be recalled. As aforementioned, the loss in robust stability margin (measured by the distance of the peak value from 1) is directly related to the sensi-

tivity of the instability to that parameter. The observed trends provide another perspective on the discussion in Subsection III B 2 on the role of these parameters, pointing at similar conclusions. In particular, it is confirmed that both parameters are more critical for the BFF instability (than for the restrained one) and that in addition the tail distance D barely affects the torsional-bending coupling (high frequency instability) which reconciles with physical understanding. Another interesting aspect that can be deduced by these results is that the effect of D on BFF is not magnified when the stiffness uncertainty level is enlarged (given that the system is flexible enough to be susceptible to BFF). This is inferred from a comparison between the *relative* increase, almost the same, in the peaks between the uncertainty level cases (from 0.58 to 0.74 for RC1-A to RC1-B, and from 1.37 to 1.7 for RC1-C to RC1-D). In other words, the bending stiffness is highly detrimental, as often mentioned in the literature, but it does not further exacerbate the influence of D (which was not so obvious prior to the μ analyses). This aspect is well connected with the curves for D = {5,6,8} in Fig. 5, which have the *same* slope (i.e. they are parallel) in the BFF region- indicating that the relative drop in flutter speed (that is, from curve to curve) is irrespective of the value of EI. Thus, it is clearly shown in Fig. 9 how μ analysis is able to provide this detailed information without requiring discrete calculations which can generally be less accurate (because no continuous guarantee exists) and more computationally expensive. It should be noted however that the results obtained with the conventional approach in Sec. III B 2 aided in providing an appropriate starting point for the insight on the μ results, i.e. they informed the selection of the LFT nominal model. This complementarity between the analyses is highly desirable and one of the novelties of the presented study.

Worst-case analysis. An additional advantage of the LFT-μ analysis framework, is that in addition to the previous sensitivity analysis, the accurate estimation of the lower bound μ_{LB} allows for the determination of the smallest critical perturbation matrix satisfying the determinant condition. In Table 2 the values of $\mathbf{\Delta_1^{cr}}$ matrices obtained at the two peak frequencies for the LFT-1 and RC1-C are reported.

It is apparent that for the first peak the instability is triggered by a *reduction* of both EI and D (negative values for δ_{EI} and δ_D), in accordance to what happens in Fig. 5 within the region where BFF is prominent. The examination of the second peak ($\mathbf{\Delta_1^{cr}}|_{\omega_2}$) reveals that a positive perturba-

tion δ_{EI} is detrimental for the restrained flutter mechanism. This is in agreement with this flutter mechanism, for which as previously commented, instability is more pronounced as the bending stiffness is increased and thus bending and torsional frequencies become closer. It is equally important to assess that the μ_{LB} is accurate in predicting the worst-case parameter combination. This can be accomplished by applying the perturbations in Table 2 to the nominal system and evaluating its eigenvalues or simulating it in the time-domain. This test is not reported here but has been applied to all the $\mathbf{\Delta^{cr}}$ matrices discussed in the work.

Table 2 Worst-case perturbations for Model 1 at the two frequency peaks

$\mathbf{\Delta_1^{cr}}$	δ_D	δ_{EI}	$\delta_{A_{12}}$	$\delta_{A_{21}}$	$\delta_{A_{22}}$
$\mathbf{\Delta_1^{cr}}\|_{\omega_1}$	-0.7622	-0.7622	-0.35-0.65i	0.37 + 0.64i	-0.67 + 0.31i
$\mathbf{\Delta_1^{cr}}\|_{\omega_2}$	-1.4156	1.4156	1.32 + 0.50i	1.1 - 0.9i	-0.72 + 1.21i

C. μ-analysis results for LFT Model 2

Parametric sensitivity study. This second LFT model (associated with $\mathbf{\Delta_2}$ in Eq. (19)) augments the previous one with an additional uncertainty, namely the wing mass ratio m_w. The sensitivity of the system's instabilities to this new parameter is studied following the same process as before. Fig. 10 shows the μ analyses, now with three different uncertainty range combinations.

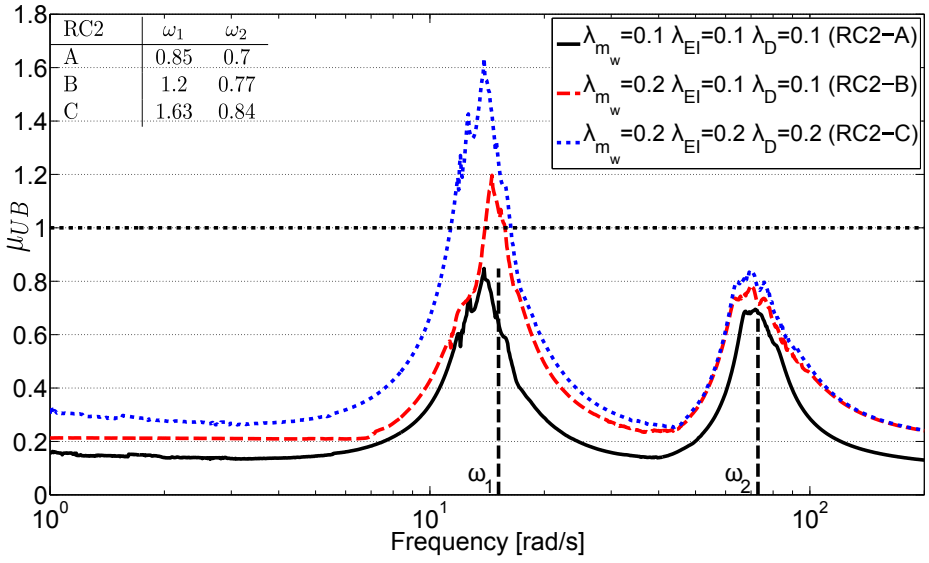

Fig. 10 μ analysis LFT-2: μ_{UB} sensitivity for different ranges (λ_{m_w},λ_{EI}, λ_D) of m_w, EI, and D.

As before, two frequency regions are observed each representing a different type of system instability (these frequencies are very close to those in Fig. 9). A comparison with the peak values in Fig. 9 for the first uncertainty level case RC2-A (solid line) reveals that the variation in mass is detrimental, particularly for the low frequency instability. The peak corresponding to the high frequency is also affected, but less markedly. The other two uncertainty level cases analyzed in Fig. 10 extend to the wing mass ratio the observations made before for the tail distance and the bending stiffness uncertain parameters. In addition, a quantitative measure of the robustness degradation is provided by the algorithm.

From further assessment of Fig. 10, it can be concluded that the m_w parameter is crucial since the BFF mode (associated with ω_1) changes from stable to unstable between RC2-A and RC2-B (δ_{m_w} from 0.1 to 0.2), while a similar switch was not observed in Fig. 9 for the other parameters until their scaling level was three times higher. Note also that the most critical instability mechanism switches again from the bending-torsional (ω_2) to the rigid-elastic (ω_1) one. Recalling from Fig. 8 that the nominal tests indicated the torsional-bending ($V_{f2} = 162.8\ \frac{m}{s}$, $\omega_{f2} = 69.7\ \frac{rad}{s}$) was the first to achieve instability with respect to the BFF ($V_{f1} = 175\ \frac{m}{s}$, $\omega_{f1} = 14.7\ \frac{rad}{s}$), now the reversal is seen in Fig. 10.

Worst-case analysis. As before, an inspection of the critical perturbations is performed next and is given in Table 3 (for RC2-B in Fig. 10).

Table 3 Worst-case perturbations for Model 2

$\mathbf{\Delta_2^{cr}}$	δ_{m_w}	δ_D	δ_{EI}	$\delta_{A_{12}}$	$\delta_{A_{21}}$	$\delta_{A_{22}}$
$\mathbf{\Delta_2^{cr}}\|_{\omega_1}$	-0.87	-0.87	-0.87	-0.35 - 0.8i	0.33 + 0.8i	-0.83 + 0.25i
$\mathbf{\Delta_2^{cr}}\|_{\omega_2}$	1.37	-1.37	1.37	1.20 + 0.65i	1.14 - 0.75i	-0.67 + 1.2i

As concerns the instability at ω_1 (i.e. BFF), the corresponding $\mathbf{\Delta^{cr}}$ confirms the trend in Table 2 for tail distance and bending stiffness, and indicates that this instability is exacerbated by a decrease in mass. The torsion-bending coupling instability (ω_2) is instead favoured by an increase in wing mass. This last effect can be ascertained by focusing solely on the interaction between the two elastic modes (similar to what was done before for $\mathbf{\Delta_1^{cr}}|_{\omega_2}$). For the BFF instability worst-case, i.e.

$\boldsymbol{\Delta}_{\mathbf{2}}^{\mathbf{cr}}|_{\omega_1}$, however, this is less straightforward than before. Nonetheless, the information provided by μ (i.e. a reduction in wing mass enhances the aircraft proneness to BFF) reconciles with known features of BFF in the literature, as was the case for D and EI. In fact, this aspect was ascribed in [3] to the effect that a lower vehicle pitch inertia I_{yy} had in increasing the short period frequency ω_{SP} (recall its expression in Eq. (7)) and thus pushing it closer to the wing bending lowest frequency. The robust (LFT and μ) flutter framework presented in here allows for the analytical ascertainment of this aspect, but crucially from a worst-case perspective, and also allowing additional relevant parameters to be included within the same analysis.

D. Reconciliation of complex physical effects via LFT modeling and μ analysis

In order to gain further insights into the mechanism prompting the instability detected by Table 3, the worst-case perturbations provided by μ for LFT Model 1 and Model 2 are exploited.

The focus of this physical reconciliation is on the dynamical properties (i.e. modes shapes and frequencies) of the two modes featuring the rigid-elastic interaction, i.e. the bending (B) and the short period (SP). The idea is to first characterize these two modes considering only the frequencies associated with the *pure* elastic and rigid modes. For the bending mode, the frequency obtained by performing a standard restrained wing analysis is considered- note that by definition this includes the aeroelastic effects of the wing but ignores its coupling with the rigid-body motion. For the short-period mode, the frequency associated with the longitudinal characteristic equation of Eq. (7), namely ω_{SP}, is employed. A second characterization is then performed evaluating these properties when the coupling terms are included.

In both cases, the monitored quantities are a function of the airspeed V, and the Modal Assurance Criteria (MAC) [31] is employed in order to associate the eigenpair (eigenvalue and eigenvector) with the two investigated modes (B and SP). The MAC algorithm enables the mode tracking problem to be addressed by quantifying the linearity between two mode shapes. This is crucial for the proposed characterizations because often a merging of the frequencies is observed in cases with strong coupling and thus a rationale to distinguish the eigenpairs is needed. The procedure adopted in this work consists of starting the analysis at a low speed such that the two modes to be tracked are distinct and well detectable. At each speed an eigenvalue analysis is performed and the tested eigenpairs are

associated with the investigated modes using the modes classified at the previous step as reference modes for the comparison. The modal reference basis is then updated and so the dynamics at the next speed can be studied.

This study is performed for four systems: System 1 (the LFT nominal); System 2 (the LFT-1 with $\delta_D = -1$, and $\delta_{EI} = -1$); System 3 (the LFT-2 with $\delta_{m_w} = -1$, $\delta_D = -1$, and $\delta_{EI} = -1$); and System 4 (the LFT-2 with $\delta_{m_w} = 1$, $\delta_D = -1$, and $\delta_{EI} = -1$). For the three parameters m_w, D, and EI an uncertainty range of 10% is considered and no aerodynamic uncertainties are included (i.e. $\delta_{A_{12}} = \delta_{A_{21}} = \delta_{A_{22}} = 0$).

This choice of systems reflects the flow of the analyses presented before. A nominal plant (System 1) was defined and starting from this a first LFT model was proposed taking into account perturbations in the wing bending flexibility EI and in the tail distance from the nose D. Results in Fig. 9 and Table 2 showed that a reduction in both the parameters is instrumental in lowering the flutter speed provoking the BFF (System 2). When wing mass is added as a varying parameter (System 3), the analysis in Fig. 10 shows again that it is the BFF mode (as opposed to the restrained wing instability) that is more susceptible to disturbances in this parameter. In order to get more insight into the physical explanation for this latter mechanism, the mass is increased from -1 (System 3, the one identified as most critical by the previous worst case analyses) to +1, yielding System 4.

Fig. 11(a) presents the first characterization (i.e. without interaction between the two modes), whereas Fig. 11(b) shows the frequencies obtained with the comprehensive model.

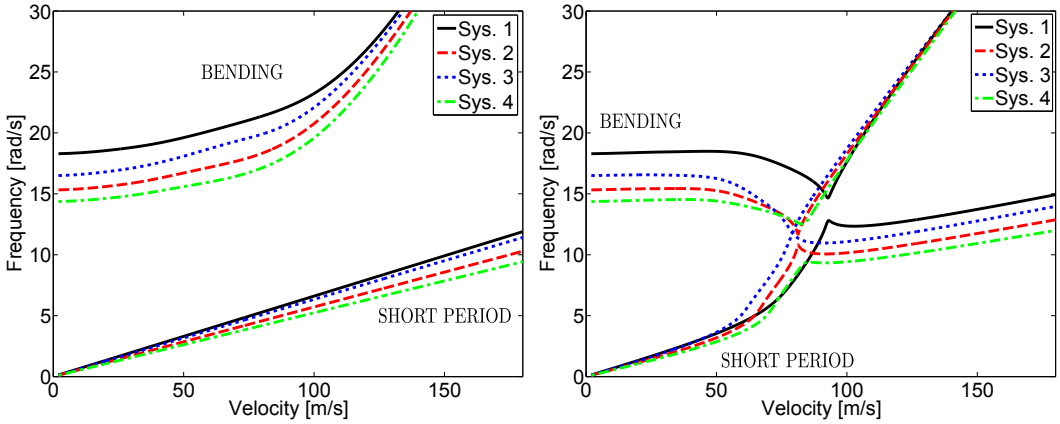

(a) Uncoupled modes

(b) Coupled modes

Fig. 11 Physical BFF modes reconciliation: frequency vs velocity

Looking at Fig. 11(a), the bending frequencies are affected by the coupling with the higher frequency torsion mode as speed increases, resulting in the observed trend. The short period frequencies instead vary linearly with flight speed and there are slight differences among the various systems due to the effect of tail distance and vehicle inertia. Note, as mentioned before, that System 3 has the highest uncoupled short-period frequency among the perturbed systems due to the effect of I_{yy}.

When Fig. 11(b) is considered, the scenario sensibly changes. As the airspeed increases (and thus the aeroelastic effects become more prominent), the frequencies are pushed away from their original values. In particular, a common trend is observed for both modes which tend to approach each other in terms of frequency values before abruptly separating. Additional features that can be detected for each system include: the speed at which the coupling gets strong enough to make the frequencies detour from their original values; the distance, in terms of frequency, reached from the original values; and a measure of the closeness of the rigid-elastic modes frequencies. All these characteristics can be seen as a qualitative measure of the strength of the rigid-elastic coupling experienced by each of the systems. System 2 and 3 seem, following the previous criteria, to be the most affected and thus a detrimental effect on their BFF stability could be expected. In fact, these two systems were found by μ analysis to be the most critically perturbed systems (among the uncertain families described by LFT 1 and LFT 2 respectively).

For the case of System 3, a unique pattern in the frequencies is also observed, since after getting close they do not *invert* their trend as do the others. As the airspeed is increased (beyond that for which the frequencies become almost coincident), the algorithm associates the frequency of the short-period mode to that expected for the bending mode (based on similarities with the trend of the other systems), and vice versa. Recalling that MAC associates the eigenpair with a reference mode by evaluating the linearity between two modes, it is inferred that the two tested eigenmodes are very *similar* (i.e. the mode shapes are almost linearly dependent). The analysis thus suggests that a coalescence of the eigenmodes is taking place, in addition to that of the frequencies. This speculation was verified a-posteriori by looking at the MAC of the two modes, which, around the speed for which the coalescence in Fig. 11(b) takes place, is approximately 1 (where MAC=1 would mean the eigenmodes are linearly dependent).

These observations, prompted by the results provided by the μ analysis, give an interesting perspective on the effect of the wing mass. The main finding is indeed that this parameter is responsible for a merging between the first bending and short-period eigenmodes. This aspect recalls previous works, such as that of reference [22], which stressed that parameters able to adversely modify the mode shapes of the aircraft are responsible for exacerbating the BFF instability.

VI. Conclusion

This article describes a dynamic aeroelastic robust stability study for flexible aircraft configurations. In order to take into account rigid-body motion and its interaction with the elastic modes, an aeroelastic model based on a straight wing and unsteady aerodynamic hypotheses is coupled with a short-period approximation of the aircraft longitudinal motion.

The key aim of the work is to demonstrate a methodology based on well-established robustness tools for the study of dynamic aeroelastic instabilities. The nominal system of the developed aeroelastic model is recast as a Linear Fractional Transformation capturing the variability (or uncertainty) of those system parameters assumed significant for stability (wing mass, tail distance and bending stiffness). The structured singular value (μ) analysis technique is then employed to perform robustness assessment for the developed LFTs. In particular, two uncertainty descriptions differing by the presence of a wing mass uncertainty parameter are studied.

The results showcase the potential of the proposed methodology and of the developed model to: [i] capture in a concise representation the dependence of the system on different parameters in a highly coupled scenario; [ii] quantitatively estimate the degradation of stability in the face of the defined uncertainties; [iii] perform a sensitivity analysis of the multiple existing instabilities to the parameters captured in the LFT; and [iv] infer further characteristics of the instabilities which can guide physical understanding. These goals were achieved by applying the robustness approach in conjunction with conventional strategies (e.g. parametric eigenvalue analysis), showing that they represent a powerful tool when used together. In this regard, examples are given of investigations prompted by findings obtained with LFT/μ and further ascertained with standard flutter analysis, and also vice versa. The advantages offered by the LFT/μ framework over standard approaches are discussed and their benefits to the understanding of the complex physical and coupled interactions

featuring BFF addressed.

It is noted that in the preliminary conceptual design stages, when typically a large number of concurrent requirements are taken into account, the proposed methodology could supply invaluable understanding of the system. In this respect, it is envisaged that these insights could inform passive means to mitigate the onset of dynamic aeroelastic instabilities. In this work, for example, trade-offs in wing stiffness, aircraft static margin, and mass are emphasized– which may substantially increase the flutter-free envelope. In a more advanced stage, when the nominal system layout is frozen, these tools can provide robustness stability and performance assessments in a time efficient way.

Appendix

The parameter values for the analyses are reported in Table 4. As detailed and motivated in Section III, the parameters defining the wing properties are derived from [18], whereas the geometric properties of the aircraft are obtained by scaling the values from [17]. As for the aerodynamic model, the Theodorsen AIC matrix $\mathbf{A}$ is tabulated in [32].

Table 4 Parameters for the flexible aircraft model

Parameter	Value	Parameter	Value
b	0.9144 m	a	-0.333
m_w	35.7187 $\frac{kg}{m}$	r_α	0.4998
x_α	0.2	ρ	1.225 $\frac{kg}{m^3}$
K_h	1.493 10^4 $\frac{N}{m^2}$	K_α	6.567 10^4 N
EI_G	9.77 10^6 $N.m^2$	GJ	9.89 10^5 Nm^2
$\bar{c}$	1.8288 m	L	12.192 m
c_t	0.3 m	L_t	2.2 m
m	1.351 10^3 kg	I_{yy}	1.4 10^3 $kg.m^2$
σ_s	0.05-1	D	5-10 m
$C^w_{L_\alpha}$,$C^t_{L_\alpha}$	2 π		

Acknowledgments

This work was funded by the European Union's Horizon 2020 research and innovation programme under grant agreement No 636307, project FLEXOP.

References

[1] Bisplinghoff, R. L. and Ashley, H., *Principles of Aeroelasticity*, Wiley, 1962.

[2] Weisshaarm, T. and Zeiler, T., "Dynamic stability of flexible forward swept wing aircraft," *Journal of Aircraft*, Vol. 20, No. 12, 1983, pp. 1014–1020.

[3] Love, M., Scott Zink, P., and Wieselmann, P., "Body Freedom Flutter of High Aspect Ratio Flying-Wings," *AIAA/ASME/ASCE/AHS/ASC Conference*, 2005.

[4] Burnett, E., Atkinson, C., Beranek, J., Sibbitt, B., Holm-Hansen, B., and Nicolai, L., "NDOF Simulation Model for Flight Control Development with Flight Test Correlation," *AIAA Modeling and Simulation Technologies Conference, Guidance, Navigation, and Control*, 2010.

[5] Cavallaro, R., Bombardieri, R., Demasi, L., and Iannelli, A., "PrandtlPlane Joined Wing: Body freedom flutter, LCO and freeplay studies," *Journal of Fluids and Structures*, Vol. 59, 2015, pp. 57 – 84.

[6] Schmidt, D., "MATLAB-Based Flight-Dynamics and Flutter Modeling of a Flexible Flying-Wing Research Drone," *Journal of Aircraft*, Vol. 53, No. 4, 2016, pp. 1045–1055.

[7] Iannelli, A., Marcos, A., and Lowenberg, M., "Modeling and Robust Body Freedom Flutter Analysis of Flexible Aircraft Configurations," *IEEE Multi-Conference on Systems and Control*, 2016.

[8] Pettit, C., "Uncertainty Quantification in Aeroelasticity: Recent Results and Research Challenges," *Journal of Aircraft*, Vol. 41, No. 5, 2004, pp. 1217–1229.

[9] Borglund, D., "The μ-k Method for Robust Flutter Solutions," *Journal of Aircraft*, Vol. 41, No. 5, 2004, pp. 1209–1216.

[10] Lind, R. and Brenner, M., "Robust Flutter Margins of an F/A-18 Aircraft from Aeroelastic Flight Data," *J. of Guidance, Control and Dynamics*, Vol. 20, No. 3, 1997, pp. 597–604.

[11] Moreno, C., Seiler, P., and Balas, G., "Model Reduction for Aeroservoelastic Systems," *Journal of Aircraft*, Vol. 51, No. 1, 2014, pp. 280–290.

[12] Bennani, S., Beuker, B., van Staveren, J., and Meijer, J., "Flutter Analysis for the F-16A/B in Heavy Store Configuration," *Journal of Aircraft*, Vol. 42, No. 6, 2005, pp. 1566–1575.

[13] Zhou, K., Doyle, J. C., and Glover, K., *Robust and Optimal Control*, Prentice-Hall, Inc., 1996.

[14] Doyle, J., "Analysis of feedback systems with structured uncertainties," *IEE Proceedings D Control Theory and Applications*, Vol. 129, No. 6, 1982, pp. 242–250.

[15] Banerjee, J., "Explicit Frequency Equation and Mode Shapes of a Cantilever Beam Coupled In Bending And Torsion," *Journal of Sound and Vibration*, 1999.

[16] Schmidt, D., *Modern flight dynamics*, McGraw-Hill, 2012.

[17] Patil, M. J., Hodges, D., and Cesnik, C., "Nonlinear Aeroelasticity and Flight Dynamics of High-Altitude Long-Endurance Aircraft," *Journal of Aircraft*, Vol. 38, No. 1, 2001, pp. 88–94.

[18] Goland, M., "The flutter of a Uniform Cantilever Wing," *Journal of Applied Mechanics*, 1945.

[19] Hassig, H. J., "An approximate True Damping Solution of the Flutter Equation by Determinant Iteration," *Journal of Aircraft*, Vol. 33, No. 7, 1971, pp. 885–889.

[20] Borello, F., Cestino, E., and Frulla, G., "Structural Uncertainty Effect on Classical Wing Flutter Characteristics," *Journal of Aerospace Engineering*, Vol. 23, No. 4, 2010, pp. 1217–1229.

[21] Weisshaar, T. and Lee, D.-H., "Aeroelastic Tailoring of Joined-Wing Configurations," *AIAA/ASME/ASCE/AHS/ASC Structures, Structural Dynamics & Materials Conference*, 2002.

[22] Beranek, J., Nicolai, L., Buonanno, M., Burnett, E., Atkinson, C., Holm-Hansen, B., and Flick, P., "Conceptual Design of a Multi-Utility Aeroelastic Demonstrator," *AIAA/ISSMO Multidisciplinary Analysis Optimization Conferences*, 2010.

[23] Marcos, A. and Balas, G., "Development of Linear Parameter Varying Models for Aircraft," *J. of Guidance, Control and Dynamics*, Vol. 27, No. 2, 2004, pp. 218–228.

[24] Mannchen, T., Bates, D., and Postlethwaite, "Modeling and Computing Worst-Case Uncertainty Combinations for Flight Control Systems Analysis," *J. of Guidance, Control and Dynamics*, Vol. 25, No. 6, 2002, pp. 1029–1039.

[25] Moulin, B., Idan, M., and Karpel, M., "Aeroservoelastic Structural and Control Optimization Using Robust Design Schemes," *J. of Guidance, Control and Dynamics*, Vol. 25, No. 1, 2002, pp. 152–159.

[26] Iannelli, A., Marcos, A., and Lowenberg, M., "Aeroelastic modeling and stability analysis: A robust approach to the flutter problem," *International Journal of Robust and Nonlinear Control*, accepted for publication, June 2017.

[27] Seiler, P., Packard, A., and Balas, G. J., "A gain-based lower bound algorithm for real and mixed μ problems," *Automatica*, Vol. 46, No. 3, 2010, pp. 493–500.

[28] Magni, J., "Linear Fractional Representation Toolbox Modelling, Order Reduction, Gain Scheduling," Technical Report TR 6/08162, DCSD, ONERA, Systems Control and Flight Dynamics, 2004.

[29] Marcos, A., Bates, D., and Postlethwaite, I., "A symbolic matrix decomposition algorithm for reduced order linear fractional transformation modelling," *Automatica*, Vol. 43, No. 7, 2007, pp. 1211 – 1218.

[30] Marcos, A., Bates, D., and Postlewhite, I., "Control oriented uncertainty modeling using μ sensitivities and skewed μ analysis tool," *IEEE Conference on Decision and Control*, 2005.

[31] Allemang, R. J. and Brown, D. L., "A correlation coefficient for modal vector analysis," *International Modal Analysis Conference*, 1982.

[32] Karpel, M., "Design for Active and Passive Flutter Suppression and Gust alleviation," Nasa Report 3482, 1981.